Journal of Materials Chemistry A

ROYAL SOCIETY OF CHEMISTRY

PAPER

View Article Online
View Journal | View Issue

Cite this: J. Mater. Chem. A, 2024, 12, 23751

Unveiling barocaloric potential in organometallic-sandwich compounds $[Cp_2M][PF_6]$ (M: Fe^{3+}, Co^{3+})†

Javier García-Ben, [a] Ignacio Delgado-Ferreiro,[a] Richard J. C. Dixey,[b] Socorro Castro-García, [a] Jorge López-Beceiro,[c] Ramon Artiaga,[c] Manuel Sánchez-Andújar, [a] Anthony E. Phillips, [b] Juan Manuel Bermúdez-García *[a] and María Antonia Señarís-Rodríguez *[a]

Organometallic-sandwich salts are well-known materials that undergo order–disorder phase transitions, leading to a high-temperature phase characterized by the total or partial disorder of ionic species. Their potential for barocaloric applications has not previously been explored. Here, we focus on two salts derived from metallocenes with the formula $[Cp_2M][PF_6]$ where Cp: cyclopentadienyl anion $(C_5H_5)^-$ and M: Fe^{3+} or Co^{3+}. These molecular salts exhibit two solid–solid phase transitions, shifting from a well-ordered crystalline phase at low temperatures to an orientationally disordered phase in the case of the Fe-compound, and a partially disordered phase in the case of the Co-compound above room temperature. We find a significant entropy change (~40 J K^{-1} kg^{-1}) and a moderate volume change (~2%) associated with these phase transitions. Additionally, we observe that these transitions are highly sensitive to external applied pressure, leading to substantial barocaloric effects (exceeding 20 K $kbar^{-1}$). Very interestingly, we obtain substantial values for reversible adiabatic temperature change (ΔT_{rev} > 10 K) under an applied pressure as low as 1 kbar, comparable to those observed in the most promising barocaloric materials. We prove that the unique structure and chemical bonding of these sandwich organometallic cations are responsible for their interesting and unusual barocaloric response. These findings position the metallocenium family as promising candidates for eco-friendly solid-state refrigeration technologies.

Received 13th May 2024
Accepted 26th July 2024

DOI: 10.1039/d4ta03310h

rsc.li/materials-a

1. Introduction

Barocaloric (BC) refrigeration is an emerging technology which takes advantage of materials typically exhibiting solid-to-solid phase transition[1] with associated large and reversible isothermal entropy changes (ΔS_{rev}), and large sensitivity to external pressure, in order to reach large barocaloric effects under low applied pressure.[2]

Over the last decade, this innovative research field has experienced significant growth. Different mechanisms of solid–solid phase transitions with barocaloric effects have been reported,[2,3] including magnetostructural, spin-crossover, ferri- and ferroelectric, lattice, order–disorder phase transitions, and even adsorption processes combined with BC effects.[4,5] A variety of materials exhibiting these transitions have been studied for barocaloric purposes. These materials encompass metal alloys,[6–22] inorganic ammonium salts,[23–26] spin-crossover materials,[27–30] superionic conductors,[31] polymers,[32–35] hybrid organic–inorganic perovskites,[36–41] and one of the most promising families for barocaloric applications, plastic crystals (PCs).[42–49]

These latter are crystalline solids composed of molecules or ions that undergo transitions involving one or more degrees of orientational freedom (order–disorder phase transitions). This transition entails a change from an organized crystalline phase to another one, wherein the molecules/ions gain rotational degrees of freedom while maintaining their central positioning within the crystalline lattice.[50] This phase transition usually involves large thermal changes, which are very attractive for barocaloric applications.

Therefore, the caloric response of various plastic crystals has been predicted and/or studied under the application of isostatic pressure.[51] Examples of these PCs include organic molecular compounds such as glycols (for example neopentylglycol and derivates),[42,45] adamantanes,[43] adamantanols[44] or hybrid coordination organic–inorganic ionic plastic crystals.[48,49,52]

[a]University of A Coruna, QUIMOLMAT Group, Dpt. Chemistry, Faculty of Science and Centro Interdisciplinar de Química e Bioloxía (CICA), Zapateira, 15071 A Coruña, Spain. E-mail: j.bermudez@udc.es; m.senaris.rodriguez@udc.es

[b]School of Physical and Chemical Sciences, Queen Mary University of London, London, E1 4NS, UK

[c]Universidade da Coruña, CITENI-Grupo Proterm, Campus Industrial de Ferrol, Campus de Esteiro, 15403 Ferrol, Spain

† Electronic supplementary information (ESI) available. See DOI: https://doi.org/10.1039/d4ta03310h

In this work, we aim to expand the flourishing family of barocaloric materials proving, for the first time in this field, the potential of the family of metallocenium salts with orientational order–disorder phase transitions in barocaloric applications.

These compounds belong to the large family of organometallic complexes, known since the XIX century,[53] which are defined as containing at least one direct metal–carbon bond in their structure. Some members of this family have played a critical role in catalysis and organic synthesis,[54] and in recent decades have received interest in new research fields such as optics,[55] biomedicine[56] or molecular magnetic devices,[57] among others.

Within the broad diversity of organometallic compounds, metallocenium salts have attracted attention for crystal engineering and molecular motion in the solid state.[58] These compounds are 'sandwich' salts with general formula $[Cp_2M][X]$ (Cp: cyclopentadienyl anion $(C_5H_5)^-$ or functionalized related rings, M: transition metal ions, X: PF_6^-, Cl^-, BF_4^-, *etc.*) (see Fig. 1).[59–63]

These compounds are known to undergo multiple and fully reversible solid-to-solid phase transitions between ordered and totally/or partially disordered phases mainly induced by the cyclopentadienyl rings, which can experience various rotational or orientational order–disorder.[62] Interestingly, these transitions can be modified depending on the chemical components, such as metal cations and anions.[64]

It is worth highlighting that this order–disorder process is different from that occurring in BC materials containing acyclic saturated long hydrocarbon chains, such as C_nH_{2n+2}, $[C_nH_{2n+2}NH_3]^+$ and $[C_nH_{2n+2}NH_2C_nH_{2n+2}]^+$, in which the hydrocarbon chains strongly disorder at the transition, giving rise to different thermally-driven chain conformers, with an associated significant large volume change, latent heat, and entropy change.[39,40,49,65]

By contrast, in metallocenium salts $[Cp_2M][X]$, the presence of π bonds in the cyclic unsaturated hydrocarbon Cp ions together with the metal–carbon bonds does not allow the presence of different conformations in the rings, preventing this disorder mechanism from occurring. Instead, the rings rotate as rigid bodies once the energy barrier to rotation is thermally overcome.[66]

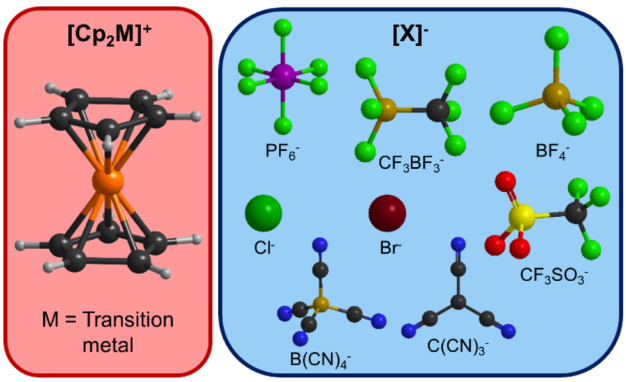

Fig. 1 Examples of cations and anions in already reported 'sandwich' $[Cp_2M][X]$ salts cations.

This orientational disorder similarly involves a relatively large latent heat and entropy change,[62] although lower than in compounds with long hydrocarbon chains. Most interestingly, the associated volume change is expected to be small, and lower than in the former. This feature enhances the cyclability of this order–disorder process, which is particularly appealing since a crucial aspect in the development of barocaloric materials is to make them reliable for long-term applications.[59,60,67]

For these reasons, in this study we explore the order–disorder mechanism present in these sandwich organometallic compounds and assess its potential for barocaloric applications.

We focus on two ionic compounds, with general formula $[Cp_2M][PF_6]$ (**1**: M = Fe^{3+}, **2**: M = Co^{3+}), to study their performance as barocaloric materials. For this purpose, we study their sensitiveness to applied pressure, their isobaric and isothermal reversible entropy changes, their reversible adiabatic temperature changes and their operating temperature ranges.

These two metallocenium salts were previously characterized in detail by Braga *et al.* in the late 90s,[60,68] who reported that both compounds experience two fully reversible solid-to-solid phase transitions near room temperature. The first transition, transforming the low temperature phase I into the isosymmetric intermediate temperature phase II (both having the monoclinic space group $P2_1/c$), is associated with a reorientation of the $[Cp_2M]^+$ cations. In the low-temperature phase, the $[Cp_2M]^+$ cations are in a staggered configuration, while above the phase transition, they undergo changes to a disordered state, with an apparent crystallographic disordered between staggered and eclipsed conformations.[59,60,66]

Meanwhile, the high temperature order–disorder transition transforms the intermediate monoclinic phase II into the cubic ($Pm\bar{3}$) phase III. In the case of compound **1**, this leads to complete orientational disorder of both cations and anions, resulting in a totally disordered phase (see Fig. 2). Meanwhile, in the case of compound **2**, there is only orientational disorder in the $[Cp_2M]^+$ cations (with the $[PF_6]^-$ anions remaining ordered), which results in a partially disordered phase.[60,68]

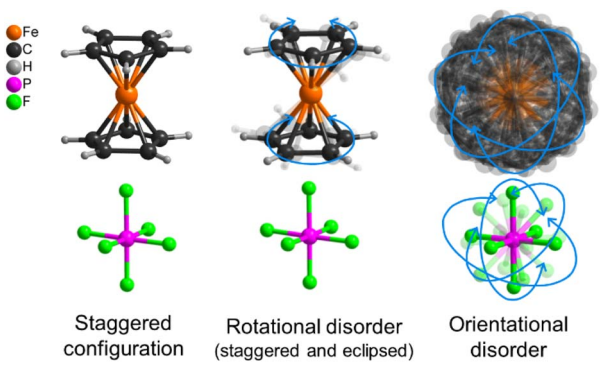

Fig. 2 Illustrating example of the dynamic evolution of the $[Cp_2Fe]^+$ cations and the $[PF_6]^-$ anions across the thermally-induced phase transitions. Note: crystal structures represented from CIF files of ref. 59.

2. Experimental

2.1. Materials and synthesis

Commercially available reagent grade $[Cp_2Co][PF_6]$ (98% Sigma-Aldrich) was directly used for these studies. Meanwhile, ferrocenium hexafluorophosphate was prepared from $[Cp_2Fe]$ (98% Sigma-Aldrich), $FeCl_3 \cdot 6H_2O$ (97% Sigma-Aldrich) and $[NH_4][PF_6]$ (99.98% Sigma-Aldrich) according to a literature procedure.[69] For this purpose, ferrocene (3.35 mmol), dissolved in water/acetone (75/25; 15 ml), was mixed with $FeCl_3 \cdot 6H_2O$ (4.5 mmol) dissolved in water (10 ml), at room temperature. The mixture was stirred for 15 min and the obtained precipitate was removed by filtration. Subsequently, NH_4PF_6 (4.45 mol) was added to the solution. Blue crystals of $[Cp_2Fe][PF_6]$ were obtained after few days upon slow evaporation of the solvent at room temperature and they were collected by filtration and washed several times with water.

2.2. Thermal analysis

Variable-temperature differential scanning calorimetric (VT-DSC) analysis at atmospheric pressure and heat capacity (C_p) measurements were carried out using a TA-Instruments Q2000 calorimeter, using heating and cooling rates of 10 K min^{-1} from 200 up to 380 K, and under a nitrogen purge of 50 ml min^{-1}. The C_p measurements were performed by following the dynamic method reported in the literature using a sapphire calibration:[70]

$$C_{pm} = Q_m C_{ps} m_s / m_m Q_s \quad (1)$$

where C_{pm} is the heat capacity of each compound, Q_m is the heat flow of these materials, C_{ps} is the heat capacity of the sapphire obtained from tabulated values, m_s is the mass of the sapphire, m_m is the mass of the material, and Q_s is the heat flow of the sapphire.

Variable-pressure differential scanning calorimetry (VP-DSC) was performed with a Setaram mDSC7 EVO microcalorimeter equipped with a 65D Isco pressure pump. Nitrogen gas was used as pressure transmitting media. Around 20 mg of sample was swept in temperature (from 320 to 390 K for compound **1**, and from 290 to 350 K for compound **2**) with heating/cooling rates of $\pm$1.2 K min^{-1} at different isobaric conditions from atmospheric pressure up to 1000 bar.

2.3. Variable-temperature synchrotron radiation powder X-ray diffraction

Variable-temperature synchrotron powder X-ray diffraction (VT-SPXRD) patterns of compounds **1** and **2** were recorded at the Diamond Synchrotron I11 beamline (Oxford, UK). A wavelength of 0.825 955(3) Å was determined by refining the positions of six individual reflections of a NIST640D silicon standard at room temperature. The samples were enclosed in a glass capillary (inner diameter ϕ = 0.5 mm) and set in continuous rotation during data collection to improve powder averaging. Patterns were collected using Mythen position sensitive detector, while heating the sample from 170 to 335 K. The working temperature was set using a FMB Oxford hot-air blower. Le Bail refinements were carried out using the program GSAS-II.[71]

2.4. Calculation of globularity

The globularity of the A-site cations (G) was calculated using the Crystal Explorer 17 software as $G = (S_{sp}/S_m)$, where S_m is the surface of the A-species while S_{sp} is the surface of a sphere of volume equal to that of the A-species volume.[72] According to this definition, G is 1.0 for a sphere, and progressively less than 1.0 as the species surface becomes more structured.

3. Results and discussion

3.1. Calorimetric and thermogravimetric analysis at atmospheric pressure

In the case of the compound **1**, the two endothermic peaks appear on heating at $T_{(I\rightarrow II)}$ ~212 K and $T_{(II\rightarrow III)}$ ~347 K and the corresponding exothermic peaks at $T_{(II\rightarrow I)}$ ~200 and $T_{(III\rightarrow II)}$ ~342 K on cooling. Meanwhile, for compound **2**, the endothermic peaks are found at $T_{(I\rightarrow II)}$ ~253 K and $T_{(II\rightarrow III)}$ ~312 K on heating, and the corresponding exothermic peaks at $T_{(II\rightarrow I)}$ ~212 K and $T_{(III\rightarrow II)}$ ~312 K on cooling (see Fig. 3).

The latent heat and entropy change associated with each phase transition, obtained from integrating under the curve of the peaks, are summarized in Table 1 and are in good agreement with previous reports.[59,60,68]

As observed, the values of latent heat and entropy change for both compounds are highest during the high-temperature phase transition. Additionally, this transition displays a lower thermal hysteresis on heating and cooling cycles compared to the lower temperature one (which is perhaps expected since the isosymmetric transition is necessarily first-order). Therefore, it will be the focus of interest for our subsequent barocaloric characterization.

As for the differences observed between the behaviour of both compounds, it should be noted that in **1** the II $\leftrightarrow$ III transition occurs at temperatures that are 35° higher (on heating) than in **2**, and with an observed increase of enthalpy and entropy changes of ~20% and ~12%, respectively.

Taking into account that for an order–disorder transition $\Delta S = R\ln(N)$, where R is the gas constant and N is the ratio of the number of configurations in the disordered and ordered system,[73] a value of $N \approx 2$ and 4.5 is calculated for compound **1** and $N \approx 2$ and 4 for compound **2**, for the I $\leftrightarrow$ II and II $\leftrightarrow$ III phase transitions, respectively. Interestingly, the difference in N of II $\leftrightarrow$ III phase transitions between both compounds could be

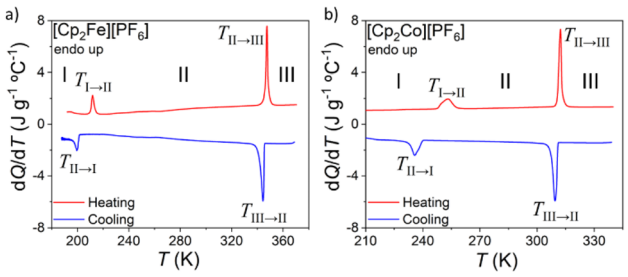

Fig. 3 VT-DSC curves on heating and cooling of (a) compound **1** between 190 and 370 K and (b) compound **2** between 210 and 340 K.

Table 1 Temperature, enthalpy and entropy change values of the observed phase transitions in compound **1** and compound **2** on heating and cooling[a]

	Compound **1**		Compound **2**	
	I ↔ II	II ↔ III	I ↔ II	II ↔ III
$T_{t(h)}$ (K)	212	347	253	312
$T_{t(c)}$ (K)	200	344	236	310
$\lvert T_{t(h)}-T_{t(c)}\rvert$	12	3	18	3
$\Delta H_{(h)}$ (kJ kg^{-1})	∼4	∼13	∼5	∼11
$\Delta H_{(c)}$ (kJ kg^{-1})	∼4	∼14	∼5	∼12
$\Delta S_{(h)}$ (J K^{-1} kg^{-1})	∼19	∼38	∼19	∼34
$\Delta S_{(h)}$ (kJ K^{-1} m^{-3})	∼36	∼69	∼36	∼64
$\Delta S_{(c)}$ (J K^{-1} kg^{-1})	∼20	∼41	∼22	∼38
$\Delta S_{(c)}$ (kJ K^{-1} m^{-3})	∼38	∼73	∼43	∼70

[a] (h) = heating, (c) = cooling.

explained due to the disordering of the $[PF_6]^-$ anion in compound **1** but not the compound **2**, as previously mentioned in the introduction.

In this context, we anticipate that by modifying the sandwich cation and/or the anion (to promote stronger or weaker interactions between them) the transition temperature could be modulated, while both ΔH and ΔS could be maximized in order to enhance the caloric performance of future materials, which is one of the main challenges for solid-state barocaloric refrigeration.

Additionally, we measured the heat capacity (C_p) of both materials, which is essential for determining certain barocaloric parameters, for a temperature range close to the observed phase transitions (see Fig. S1 of ESI† which represents the heat capacity of both materials as a function of temperature). Their C_p values are relatively low, as also reported for other sandwich-type compounds.[74–78] Compound **2** presents higher C_p than **1**: C_p (phase I) ∼820 (compound **1**) and ∼1100 J per °C per kg (compound **2**); C_p (phase II) ∼1260 (**1**) and ∼1350 J per °C per kg (**2**); C_p (phase III) ∼1280 (**1**) and ∼1540 J per °C per kg (**2**), differences which could be related to the extra stability of compound **2**, with stronger intramolecular interactions.

Very interestingly, these values are lower than other reported barocaloric materials with order–disorder phase transitions as organic plastic crystals such as neopentylglycol (C_p ∼ [1600–2600] J per °C per kg),[42] and than hybrid materials such as the layered hybrid perovskite $[C_{12}H_{21}NH_3]_2[MnCl_4]$ (C_p ∼ [1500–1800] J per °C per kg), materials with much larger internal mobility in their species or alkyl chains than the cyclopentadienyl rings of the organometallic 'sandwich' salts.

The heat capacity of compound **1** is more similar to that of fullerite (C_{60}) (C_p ∼ [650–900] J per °C per kg),[46] as expected since these species are even more rigid than the sandwich cations.[79]

In the particular case of these organometallic complexes, we suggest that their low C_p can be attributed *inter alia* to the robust bonding between M–C of cyclopentadienyl rings and π bonds between the carbon atoms. These bonds restrict the vibrational modes of the cyclopentadienyl rings, imparting exceptional stiffness to the entire organometallic complex. The chemical bonds confine atomic motions outside the plane of the ring, while allowing the entire ring to rotate in its plane.

From thermogravimetric analysis, compound **2** presents higher thermal stability (with a decomposition temperature of T_d ∼650 K) than compound **1** (with T_d ∼450 K) (see Fig. S2 of ESI†). This could be related to the fact that, in compound **2**, the $[Cp_2Co]^+$ cation obeys the 18 e$^-$ rule,[80] while the Fe-sandwich does not, resulting in stronger bonds and shorter M–C distances in the cation.[59,60,66]

3.2. Barocaloric properties estimated by indirect methods: Clausius–Clapeyron

The indirect method using Clausius–Clapeyron equation allows one to estimate the barocaloric coefficient (dT_t/dp):

$$dT_t/dp = \Delta V/\Delta S \quad (2)$$

where ΔV is the volume change between two different polymorphs at the phase transition, and ΔS can be obtained from the value of the phase transition entropy change (see Table 1).

In order to calculate the different ΔV values across the phase transitions, we perform variable-temperature synchrotron powder X-ray diffraction (VT-SPXRD). The cell parameters were obtained by Le Bail refinement (see Fig. 4 and S3–S5 of ESI†). Two sharp structural changes occur at $T_{(I\rightarrow II)}$ ∼211 K and $T_{(II\rightarrow III)}$ ∼350 K for compound **1**, and at $T_{(I\rightarrow II)}$ ∼258 K and $T_{(II\rightarrow III)}$ ∼315 K for compound **2**. These values are in excellent agreement with those observed by VT-DSC. There is not only a perfect match of the temperature at which the two transitions occur, but the enthalpy and height of the heat flow peaks are proportional to the unit volume jumps observed by VT-SPXRD.

Regarding the volume evolution over temperature, both compounds exhibit a conventional positive thermal expansion upon heating and an abrupt volume change associated with each phase transition, an effect which is larger in the case of the II–III phase transition: $\Delta V_{I\rightarrow II}$ ∼1.22% (compound **1**) and 1.27% (compound **2**), while $\Delta V_{II\rightarrow III}$ ∼2.24% (compound **1**) and 2.02% (compound **2**). Remarkably, the change in volume $\Delta V_{II\rightarrow III}$ is quite similar in both compounds, despite the fact that compound **1** exhibits disorder in both anions and cations, while compound **2** only shows disorder in the cations.[59,60] Consequently, we can infer that most of the observed volume increase

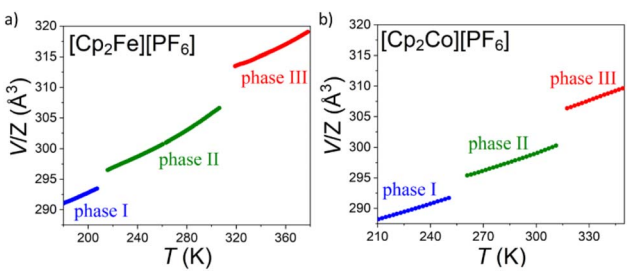

Fig. 4 Thermal evolution of unit-cell volume per formula unit of (a) compound **1** and (b) compound **2**.

at phase transition is likely associated with the disordering of the $[Cp_2M]^+$ cations. As mentioned earlier, the intramolecular bonds in $[Cp_2M]^+$ cations strongly restrict the degrees of freedom of Cp anions.[59,60,66,68] Specifically, in phase III, there is a rotation of Cp rings within their planes (similar to phase II), and additionally, the rotational axis is no longer fixed; it can rotate in any direction around the metal cation. This change leads to a significant increase in volume ($\Delta V \sim 2\%$) associated with the high-temperature phase transition, even if significantly lower than that reported for barocaloric materials with acyclic saturated long hydrocarbon chains, typically around $\Delta V \sim 7\%$.[40,49] It's important to note that in first-order-type barocaloric materials,[81] the pressure-sensitiveness (barocaloric coefficient) will be maximized for larger volume changes and lower entropy changes. Nevertheless, for practical applications, a lower volume change will reduce mechanical fatigue, ensuring a long functional lifetime, meanwhile a larger entropy change will provide a larger barocaloric effect. Therefore, it is important to reach a compromise between volume changes and entropy changes considering any each specific application and/or device.

To try to understand if this smaller variation of volume is related to the shape of the ionic molecular species, we have calculated the globularity (G) of both the cations and the anions, obtaining values of G(cations) = 0.89 and G(anions) = 0.92. It is important to note that G is 1.0 for a perfect sphere and decreases progressively as the species surface becomes more structured.[72] Therefore, both ionic molecular species exhibit only a slight distortion from spherical morphology. Consequently, the orientational disorder of these species does not cause a significant increase in volume, as confirmed experimentally. This could be improved by modifying the cations and anions by others more anisotropic, which could lead to higher entropy changes also.

From the VT-SPXRD data and the previous VT-DSC results, we focus on the high-temperature transitions of these compounds to estimate their barocaloric coefficient by indirect methods. We find values of $dT_t/dp \sim 34.1$ K kbar^{-1} and 29.7 K kbar^{-1}, for compounds **1** and **2**, respectively.

3.3. Barocaloric properties by quasi-direct methods under isobaric conditions

In order to experimentally study the barocaloric properties of $[Cp_2M][PF_6]$ (M = Fe^{3+}, Co^{3+}) related to the higher temperature (and more energetic) transitions, we carried out VT-DSC measurements under different isobaric conditions from 1 to 1000 bar.

As it can be seen in Fig. 5, the transition temperature of both compounds shifts towards higher temperatures when increasing the pressure, which is indicative of a conventional barocaloric effect.

Accordingly, the studied compounds show an experimental barocaloric coefficient as large as $dT/dp \sim 27.6$ K kbar^{-1} and ~ 24.0 K kbar^{-1} for compounds **1** and **2**, respectively. These values are slightly smaller than those estimated by Clausius–Clapeyron. Nevertheless, they still lie among the largest

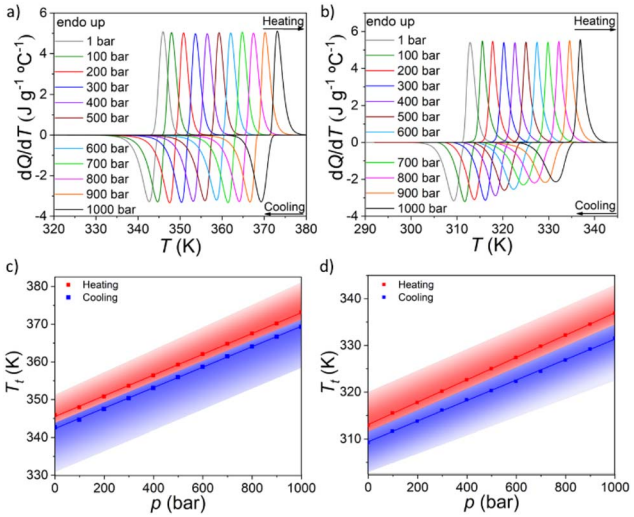

Fig. 5 VT-DSC curves at different pressures for (a) compound **1** and (b) compound **2**. Transition temperature dependence with pressure for (c) compound **1** and (d) compound **2**. Note: solid points indicate the peak maximums, solid lines represent, and shaded areas represent the peak width from the onset to the offset of the peaks. Red = heating data, blue = cooling data.

reported values (see Table S1 of ESI†), similar to some of most sensitive to pressure plastic crystals as 1-chloroadamantane ($dT/dp \sim 27.4$ K kbar^{-1}), *o*-carborane ($dT/dp \sim 30.0$ K kbar^{-1}) or dibutylammonium tetrafluoroborate ($dT/dp \sim 28.9$ K kbar^{-1}), and significantly higher than the fullerite mentioned before ($dT/dp \sim 17.0$ K kbar^{-1}). This fact indicates the large pressure sensibility of these family of organometallic sandwich-type materials.[2]

In addition, we have calculated the barocaloric effects in terms of isothermal entropy change ($\Delta S_{it(q-d)}$) as the difference between the entropy change at different isobaric conditions (ΔS_{ib}):[40,82]

$$\Delta S_{ib} = S(T_f, p) - S(T_0, p) = \int_{T_0}^{T_f} \frac{1}{T}\left[C_p(T, p_{atm}) + \frac{dQ}{dT}(T, p)\right]dT \quad (3)$$

$$\Delta S_{it(q-d)} = \Delta S_{ib}(p \neq 1, T) - \Delta S_{ib}(p = 1, T) \quad (4)$$

where T_0 and T_f are the starting and end temperature chosen arbitrary ($T_0 = 200$ K and $T_f = 380$ K for both compounds), p is the constant pressure of each isobaric curve, p_{atm} is atmospheric pressure and C_p is the heat capacity of the material for each temperature at atmospheric pressure, which is considered independent from the applied pressure.

The curves obtained for ΔS_{ib} and $\Delta S_{it(q-d)}$ can be observed in Fig. S6 of ESI† and 6, respectively. Here, $\Delta S_{it(q-d)}$ values already take into account the additional entropy change ($\Delta S_{ad(p)}$) that arises from the material's thermal expansion separately from the phase transition (see Fig. S7 and S8 of ESI†), as calculated by eqn (5):[42,83,84]

$$\Delta S_{ad(p)} = -[m^{-1}(\delta V/\delta T)_{p_{atm}}](p - p_{atm}) \quad (5)$$

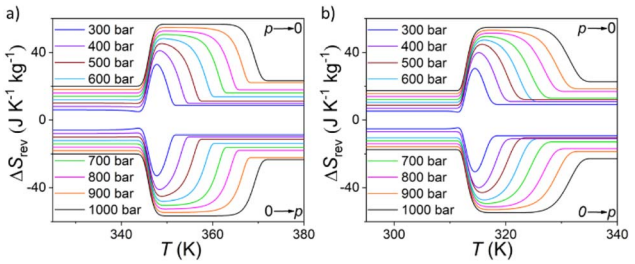

Fig. 6 Reversible pressure-driven isothermal entropy changes on applying (0 → p) and removing (p → 0) pressure of (a) compound **1** and (b) compound **2**.

where m is the cell mass of the material, $(\delta V/\delta T)_{p_{atm}}$ is the volumetric thermal expansion of the unit cell and p is the applied pressure. This approximation considers the thermal expansion to be independent of the applied pressure, which would be only valid for materials with relatively low compressibility. In the case of extremely compressible materials, this approximation can result in an overestimation of the barocaloric effects.

The as-calculated $|\Delta S_{ad}|$ show similar values for both compounds of around [17–19] J K^{-1} kg^{-1} at 1000 bar, which are a very significant contribution to the final barocaloric effects, as they represent around (33–36)% of the total entropy change at this pressure.

Considering this additional contribution, the barocaloric effects at 1000 bar are as large as $\Delta S_{it(rev)}$ ~57 J K^{-1} kg^{-1}, and ~55 J K^{-1} kg^{-1} for compound **1** and **2**, respectively (see Fig. 6 and S9 of ESI†).

Very interestingly, these compounds can also exhibit relatively large barocaloric effects, even larger than the previously mentioned fullerite (~25 J K^{-1} kg^{-1} under 1000 bar),[46] of around ~30 J K^{-1} kg^{-1} in a reversible way under the application of much lower pressures of 300 bar, which is the operating pressure limit recommended by barocaloric technological roadmaps to enhance energy efficiency.[85]

In addition, we have calculated the adiabatic temperature change (ΔT) (see Fig. 7 and S10 of ESI†):

$$|\Delta T(S;p_{atm} \leftrightarrow p)| = |T(S;p) - T(S;p_{atm})|\Delta T = -(T/C_p)\Delta S_{it} \quad (6)$$

In this context, it's worth noting that the adiabatic temperature change is directly proportional to the reversible entropy change and inversely proportional to the heat capacity. Adiabatic temperature change refers to the temperature variation experienced by a barocaloric material when pressure is applied and removed adiabatically. Consequently, this parameter holds immense importance for practical applications and is considered one of the most critical factors for evaluating the performance of barocaloric materials.

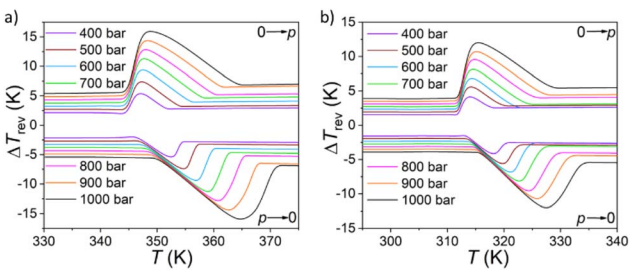

Fig. 7 Reversible adiabatic temperature changes on applying (0 → p) and removing (p → 0) pressure for (a) compound **1** and (b) compound **2**.

As shown in Fig. 7, these compounds present rather high values of ΔT_{rev} ~16 K (compound **1**) and ~12 K (compound **2**) at 1000 bar. This significant ΔT_{ad} is a result of a combination of moderately large entropy change and low heat capacity, factors linked to the unique molecular geometry and chemical bonding of the sandwich organometallic cations.

Also, we have represented the operating temperature range or temperature span (T_{span}) of these compounds as a function of the applied pressure, including the reversible isothermal entropy changes (Fig. 8a and b) and the reversible adiabatic temperature changes (Fig. 8c and d) that can be achieved. Compounds **1** and **2** under 1000 bar present a large operating temperature range of 17 K (with ΔS_{it} ~35 J K^{-1} kg^{-1}, ΔT_{rev} ~6 K) and of 20 K (with ΔS_{it} ~35 J K^{-1} kg^{-1}, ΔT_{rev} ~6 K).

The fullerite, which exhibits the same type of disorder as the organometallic salts reported here, rotational disorder, presents an operating temperature range as large as 11 K, showing values of $\Delta S_{it} = 25$ J K^{-1} kg^{-1} and $\Delta T_{rev} = 5$ K under a pressure of 1000 bar.

Finally, we compare the barocaloric behaviour of these compounds with other barocaloric materials (see Fig. 9 and Table S1 of ESI†). Those values obtained are considerable high compared with those of many other reported barocaloric materials, reflecting the large pressure sensibility of these family of organometallic sandwich-type materials (see Fig. 9a). These results indicate a large pressure sensibility of these family of organometallic sandwich-type materials.[2] On the other hand,

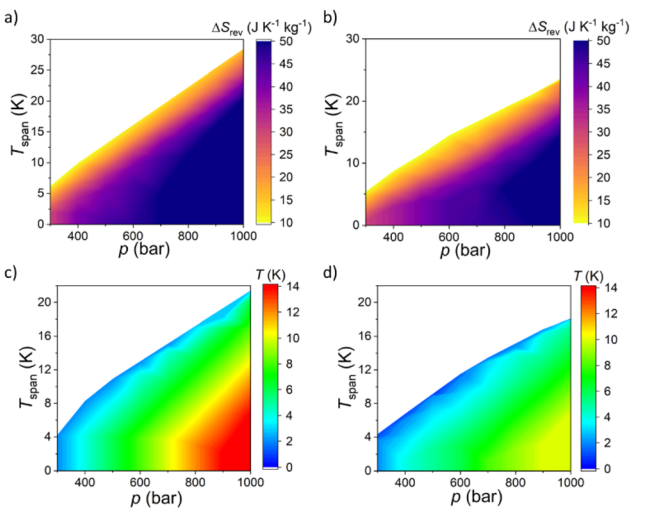

Fig. 8 Temperature span as a function of applied pressure for different intervals of reversible isothermal entropy changes, for (a) compound **1** and (b) compound **2**. And temperature span as a function of applied pressure for different intervals of reversible adiabatic temperature changes for (c) compound **1** and (d) compound **2**.

these organometallic compounds exhibit values of $\Delta S_{it(rev)}$ relatively lower than those of other BC materials (see Fig. 9b). In the same line, the obtained values of ΔT_{rev} for these compounds are already very similar to most of reported barocaloric materials, even if these are the first examples of organometallic barocaloric materials and they still have range for improvement (see Fig. 9c).

Therefore, these two cyclopentadienyl organometallic compounds show promising barocaloric parameters, which encourage further exploration of more members of this family for barocaloric applications.

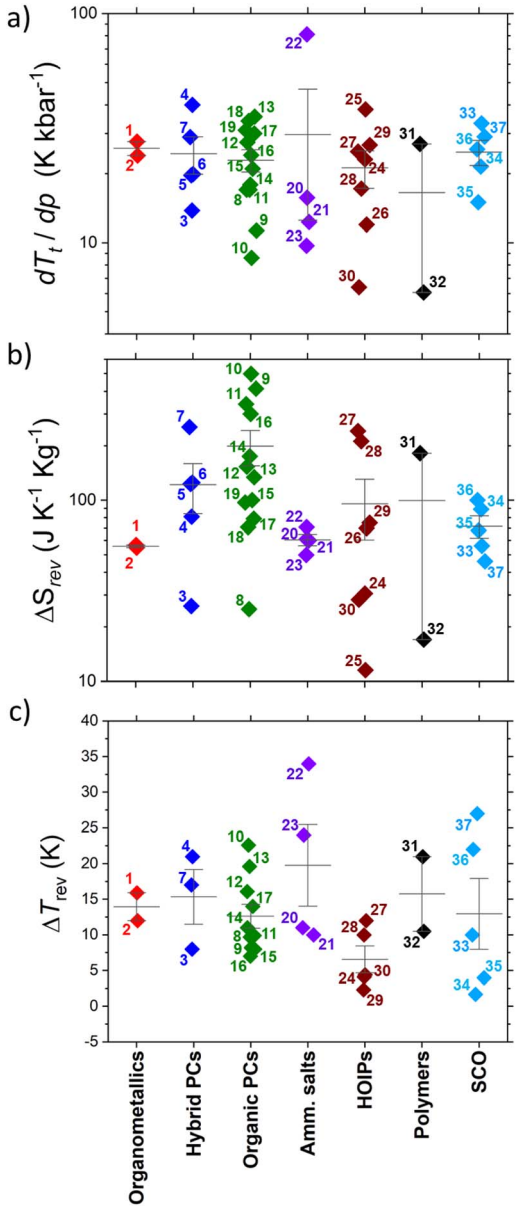

Fig. 9 Main caloric parameters of compounds **1** and **2** in comparison with a selection of the best barocaloric materials known up to date: (a) barocaloric coefficient, (b) reversible isothermal entropy change and (c) adiabatic reversible temperature change. Note: the black lines represent the average value and its error. Note 2: more information about all the materials showed in the figure can be found in Table S1 of ESI† and in the references.

4. Conclusions

In this study, we report new properties that bring about new applications for relatively "old" and well-established compounds, namely, the metallocenium salts $[Cp_2M][PF_6]$ (M = Fe^{3+}, Co^{3+}). These salts undergo two reversible order–disorder solid–solid phase transitions, one of which occurs above room temperature and show enough entropy change for barocaloric applications. The high-temperature transition is more significant than the other in terms of rotational motions, where the cations and/or anions experience a substantial increase in their orientational disorder. Although the value of ΔS ~40 J K^{-1} kg^{-1} associated with the PC transition is moderate at ambient pressure, the elastic contribution under moderate pressure (below 1000 bar) amplifies these values to $\Delta S_{it(rev)}$ ~57 J K^{-1} kg^{-1}, and ~55 J K^{-1} kg^{-1} for compound **1** (Fe) and **2** (Co), respectively. Even more interestingly, these organometallic compounds exhibit remarkably large barocaloric coefficients of dT_t/dp ~30 K kbar^{-1}, wide operating temperature ranges of $T_{span} \geq 15$ at 1000 bar, and surprisingly substantial adiabatic temperature changes, ΔT_{rev} of 12–16 K (which accounts for around 35% of the total entropy change). This latter feature can be attributed to the relatively low heat capacity found in both compounds.

Therefore, these materials offer a combination of interesting properties for practical applications, notably the moderate values reversible adiabatic temperature change, high sensitivity to applied pressure, and small volume change associated with the phase transition. We propose that the unique structure and chemical bonding of these sandwich organometallic cations are responsible for their fascinating and unusual barocaloric response, which we anticipate can be tuned by modifying shape and the globularity of their ions. These findings place the metallocenium family as promising candidates for eco-friendly solid-state refrigeration technologies.

Data availability

The data supporting this article have been included as part of the ESI.† For additional information, please contact the corresponding authors.

Author contributions

J. G.-B. was involved in all of the experimental work. S. C.-G., M. S.-A., J. M. B.-G. and M. A. S.-R. conceived the project. R. J. C. D. and A. E. P. were involved in VT-SPXRD and high-pressure DSC experiments. M. S.-A. and I. D.-F. were involved in VT-SPXRD experiments. J. L.-B. and R. A. were involved in low-pressure DSC and C_p calculations. All authors were involved in the discussion of results and in the manuscript writing and revision. M. S.-A., J. M. B.-G. and M. A. S.-R. directed and supervised this project.

Conflicts of interest

There are no conflicts to declare.

Acknowledgements

The authors thank financial support from grant PID2021-122532OB-I00 funded by MCIN/AEI/10.13039/501100011033 and ERDF A way of making Europe, the project PDC2021-121076-I00 funded by MCIN/AEI/10.13039/501100011033 and by the European Union Next GenerationEU/PRTR, and the projects ED431C 2022/39 and ED431F 2023/33 funded by Xunta de Galicia. This publication is part of the grant RYC2021-033040-I, funded by MCIN/AEI/10.13039/501100011033 and from European Union «NextGenerationEU»/PRTR». J. G. B. thanks Xunta de Galicia for postdoctoral fellowship ED481B/2024. J. M. B. G. is grateful for the support received by UDC-Inditex InTalent Programme. R. J. C. D. and A. E. P. would like to thank the financial support of EPSRC throughout provision of the funding (EP/S03577X/1). The authors thank Diamond Light Source for the award of beamtime (CY30448-1 on I11), and Eamonn Connolly for his assistance on the experiment.

Notes and references

1 P. Lloveras, *Barocaloric Effects in the Solid State – Materials and Methods*, 2023.
2 P. Lloveras and J.-L. Tamarit, *MRS Energy Sustain.*, 2021, **8**, 3–15.
3 D. Boldrin, *Appl. Phys. Lett.*, 2021, **118**, 170502.
4 J. García-Ben, J. López-Beceiro, R. Artiaga, J. Salgado-Beceiro, I. Delgado-Ferreiro, Y. V. Kolen'ko, S. Castro-García, M. A. Señarís-Rodríguez, M. Sánchez-Andújar and J. M. Bermúdez-García, *Chem. Mater.*, 2022, **34**, 3323–3332.
5 M. Gelpi, J. García-Ben, S. Rodríguez-Hermida, J. López-Beceiro, R. Artiaga, Á. Baaliña, M. Romero-Gómez, J. Romero-Gómez, S. Zaragoza, J. Salgado-Beceiro, J. Walker, C. J. McMonagle, S. Castro-García, M. Sánchez-Andújar, M. A. Señarís-Rodíguez and J. M. Bermúdez-García, *Adv. Mater.*, 2024, **36**, 2310499.
6 A. Aznar, A. Gràcia-Condal, A. Planes, P. Lloveras, M. Barrio, J. L. Tamarit, W. Xiong, D. Cong, C. Popescu and L. Mañosa, *Phys. Rev. Mater.*, 2019, **3**, 1–7.
7 L. Mañosa, D. González-Alonso, A. Planes, E. Bonnot, M. Barrio, J. L. Tamarit, S. Aksoy and M. Acet, *Nat. Mater.*, 2010, **9**, 478–481.
8 D. Matsunami, A. Fujita, K. Takenaka and M. Kano, *Nat. Mater.*, 2015, **14**, 73–78.
9 Z. Wei, Y. Shen, Z. Zhang, J. Guo, B. Li, E. Liu, Z. Zhang and J. Liu, *APL Mater.*, 2020, **8**, 051101.
10 E. Stern-Taulats, A. Planes, P. Lloveras, M. Barrio, J. L. Tamarit, S. Pramanick, S. Majumdar, S. Yüce, B. Emre, C. Frontera and L. Mañosa, *Acta Mater.*, 2015, **96**, 324–332.
11 E. Stern-Taulats, A. Planes, P. Lloveras, M. Barrio, J. L. Tamarit, S. Pramanick, S. Majumdar, C. Frontera and L. Mañosa, *Phys. Rev. B: Condens. Matter Mater. Phys.*, 2014, **89**, 1–8.
12 R. R. Wu, L. F. Bao, F. X. Hu, H. Wu, Q. Z. Huang, J. Wang, X. L. Dong, G. N. Li, J. R. Sun, F. R. Shen, T. Y. Zhao, X. Q. Zheng, L. C. Wang, Y. Liu, W. L. Zuo, Y. Y. Zhao, M. Zhang, X. C. Wang, C. Q. Jin, G. H. Rao, X. F. Han and B. G. Shen, *Sci. Rep.*, 2015, **5**, 1–11.
13 X. J. He, K. Xu, S. X. Wei, Y. L. Zhang, Z. Li and C. Jing, *J. Mater. Sci.*, 2017, **52**, 2915–2923.
14 X. He, Y. Kang, S. Wei, Y. Zhang, Y. Cao, K. Xu, Z. Li, C. Jing and Z. Li, *J. Alloys Compd.*, 2018, **741**, 821–825.
15 L. Mañosa, D. González-Alonso, A. Planes, M. Barrio, J. L. Tamarit, I. S. Titov, M. Acet, A. Bhattacharyya and S. Majumdar, *Nat. Commun.*, 2011, **2**, 1–5.
16 D. Boldrin, E. Mendive-Tapia, J. Zemen, J. B. Staunton, T. Hansen, A. Aznar, J. L. Tamarit, M. Barrio, P. Lloveras, J. Kim, X. Moya and L. F. Cohen, *Phys. Rev. X*, 2018, **8**, 41035.
17 S. Yuce, M. Barrio, B. Emre, E. Stern-Taulats, A. Planes, J. L. Tamarit, Y. Mudryk, K. A. Gschneidner, V. K. Pecharsky and L. Mañosa, *Appl. Phys. Lett.*, 2012, **101**, 071906.
18 J. Lin, P. Tong, X. Zhang, Z. Wang, Z. Zhang, B. Li, G. Zhong, J. Chen, Y. Wu, H. Lu, L. He, B. Bai, L. Ling, W. Song, Z. Zhang and Y. Sun, *Mater. Horiz.*, 2020, **7**, 2690–2695.
19 X. He, S. Wei, Y. Kang, Y. Zhang, Y. Cao, K. Xu, Z. Li and C. Jing, *Scr. Mater.*, 2018, **145**, 58–61.
20 E. Stern-Taulats, A. Gràcia-Condal, A. Planes, P. Lloveras, M. Barrio, J. L. Tamarit, S. Pramanick, S. Majumdar and L. Mañosa, *Appl. Phys. Lett.*, 2015, **107**, 152409.
21 H. Liu, Z. Li, Y. Zhang, Z. Ni, K. Xu and Y. Liu, *Scr. Mater.*, 2020, **177**, 1–5.
22 P. Lloveras, T. Samanta, M. Barrio, I. Dubenko, N. Ali, J. L. Tamarit and S. Stadler, *APL Mater.*, 2019, **7**, 9.
23 M. V. Gorev, E. A. Mikhaleva, I. N. Flerov and E. V. Bogdanov, *J. Alloys Compd.*, 2019, **806**, 1047–1051.
24 M. V. Gorev, E. V. Bogdanov, I. N. Flerov, V. N. Voronov and N. M. Laptash, *Ferroelectrics*, 2010, **397**, 76–80.
25 M. V. Gorev, E. V. Bogdanov, I. N. Flerov, A. G. Kocharova and N. M. Laptash, *Phys. Solid State*, 2010, **52**, 167–175.
26 Q. Ren, J. Qi, D. Yu, Z. Zhang, R. Song, W. Song, B. Yuan, T. Wang, W. Ren, Z. Zhang, X. Tong and B. Li, *Nat. Commun.*, 2022, **13**, 1–9.
27 S. P. Vallone, A. N. Tantillo, A. M. dos Santos, J. J. Molaison, R. Kulmaczewski, A. Chapoy, P. Ahmadi, M. A. Halcrow and K. G. Sandeman, *Adv. Mater.*, 2019, **31**, 1–7.
28 P. J. Von Ranke, B. P. Alho, R. M. Ribas, E. P. Nobrega, A. Caldas, V. S. R. De Sousa, M. V. Colaço, L. F. Marques, D. L. Rocco and P. O. Ribeiro, *Phys. Rev. B*, 2018, **98**, 2–6.
29 M. Romanini, Y. Wang, G. Kübra, G. Ornelas, P. Lloveras, Y. Zhang, W. Zheng, M. Barrio, A. Aznar, A. Gràcia-Condal, B. Emre, O. Atakol, C. Popescu, H. Zhang, Y. Long, L. Balicas, J. L. Tamarit, A. Planes, M. Shatruk and L. Mañosa, *Adv. Mater.*, 2021, **33**, 2008076.
30 J. Seo, J. D. Braun, V. M. Dev and J. A. Mason, *J. Am. Chem. Soc.*, 2022, **144**, 6493–6503.
31 A. Aznar, P. Lloveras, M. Romanini, M. Barrio, J. L. Tamarit, C. Cazorla, D. Errandonea, N. D. Mathur, A. Planes, X. Moya and L. Mañosa, *Nat. Commun.*, 2017, **8**, 1851.
32 W. Imamura, É. O. Usuda, L. S. Paixão, N. M. Bom, A. M. Gomes and A. M. G. Carvalho, *Chin. J. Polym. Sci.*, 2020, **38**, 999–1005.

33 A. M. G. Carvalho, W. Imamura, E. O. Usuda and N. M. Bom, *Eur. Polym. J.*, 2018, **99**, 212–221.
34 J. R. Bocca, S. L. Favaro, C. S. Alves, A. M. G. Carvalho, J. R. Barbosa, A. dos Santos, F. C. Colman, W. A. do. S. Conceição, C. Caglioni and E. Radovanovic, *Polym. Test.*, 2021, **100**, 107251.
35 E. O. Usuda, N. M. Bom and A. M. G. Carvalho, *Eur. Polym. J.*, 2017, **92**, 287–293.
36 J. M. Bermúdez-García, M. Sánchez-Andújar, S. Castro-García, J. López-Beceiro, R. Artiaga and M. A. Señarís-Rodríguez, *Nat. Commun.*, 2017, **8**, 15715.
37 J. M. Bermúdez-García, S. Yáñez-Vilar, A. García-Fernández, M. Sánchez-Andújar, S. Castro-García, J. López-Beceiro, R. Artiaga, M. Dilshad, X. Moya and M. A. Señarís-Rodríguez, *J. Mater. Chem. C*, 2018, **6**, 9867–9874.
38 J. Salgado-Beceiro, A. Nonato, R. X. Silva, A. García-Fernández, M. Sánchez-Andújar, S. Castro-García, E. Stern-Taulats, M. A. Señarís-Rodríguez, X. Moya and J. M. Bermúdez-García, *Mater. Adv.*, 2020, **1**, 3167–3170.
39 Y. Gao, H. Liu, F. Hu, H. Song, H. Zhang, J. Hao, X. Liu, Z. Yu, F. Shen, Y. Wang, H. Zhou, B. Wang, Z. Tian, Y. Lin, C. Zhang, Z. Yin, J. Wang, Y. Chen, Y. Li, Y. Song, Y. Shi, T. Zhao, J. Sun, Q. Huang and B. Shen, *NPG Asia Mater.*, 2022, **14**, 34.
40 J. Li, M. Barrio, D. J. Dunstan, R. Dixey, X. Lou, J. L. Tamarit, A. E. Phillips and P. Lloveras, *Adv. Funct. Mater.*, 2021, **31**, 1–8.
41 C. Escorihuela-Sayalero, L. C. Pardo, M. Romanini, N. Obrecht, S. Loehlé, P. Lloveras, J. -L- Tamarit and C. Cazorla, *npj Comput. Mater.*, 2024, **10**, 13.
42 P. Lloveras, A. Aznar, M. Barrio, P. Negrier, C. Popescu, A. Planes, L. Mañosa, E. Stern-Taulats, A. Avramenko, N. D. Mathur, X. Moya and J. L. Tamarit, *Nat. Commun.*, 2019, **10**, 1–7.
43 A. Aznar, P. Negrier, A. Planes, L. Mañosa, E. Stern-Taulats, X. Moya, M. Barrio, J. L. Tamarit and P. Lloveras, *Appl. Mater. Today*, 2021, **23**, 101023.
44 A. Salvatori, P. Negrier, A. Aznar, M. Barrio, J. L. Tamarit and P. Lloveras, *APL Mater.*, 2022, **10**, 111117.
45 A. Aznar, P. Lloveras, M. M. Barrio, P. Negrier, A. Planes, L. L. Mañosa, N. D. Mathur, X. Moya and J. L. L. Tamarit, *J. Mater. Chem. A*, 2020, **8**, 639–647.
46 J. Li, D. Dunstan, X. Lou, A. Planes, L. Mañosa, M. Barrio, J. L. Tamarit and P. Lloveras, *J. Mater. Chem. A*, 2020, **8**, 20354–20362.
47 K. Zhang, R. Song, J. Qi, Z. Zhang, Z. Zhang, C. Yu, K. Li, Z. Zhang and B. Li, *Adv. Funct. Mater.*, 2022, **32**, 2112622.
48 A. Salvatori, D. Aguilà, G. Aromí, L. Mañosa, A. Planes, P. Lloveras, L. C. Pardo, M. Appel, G. F. Nataf, F. Giovannelli, M. Barrio, J. L. Tamarit and M. Romanini, *J. Mater. Chem. A*, 2023, **11**, 12140–12150.
49 J. Garcia-Ben, J. M. Bermúdez-García, R. J. C. Dixey, I. Delgado-Ferreiro, A. L. Llamas-Saiz, J. López-Beceiro, R. Artiaga, A. Garcia-Fernandez, U. B. Cappel, B. Alonso, S. Castro-Garcia, A. E. Phillips, M. Sánchez-Andújar and M. A. Señarís-Rodríguez, *J. Mater. Chem. A*, 2023, **11**, 22232–22247.
50 L. A. K. Staveley, *Annu. Rev. Phys. Chem.*, 1962, **13**, 351–368.
51 S. Das, A. Mondal and C. M. Reddy, *Chem. Soc. Rev.*, 2020, **49**, 8878–8896.
52 J. Salgado-Beceiro, J. M. Bermúdez-García, E. Stern-Taulats, J. García-Ben, S. Castro-García, M. Sánchez-Andújar, X. Moya and M. A. Señarís-Rodríguez, *ChemRxiv*, 2021, 17–19.
53 L. B. Hunt, *Platinum Met. Rev.*, 1984, **28**, 76–83.
54 W. A. Herrmann, *Angew. Chem., Int. Ed.*, 2002, **41**, 1290–1309.
55 H. S. Nalwa, *Appl. Organomet. Chem.*, 1991, **5**, 349–377.
56 C. S. Allardyce, A. Dorcier, C. Scolaro and P. J. Dyson, *Appl. Organomet. Chem.*, 2005, **19**, 1–10.
57 R. A. Layfield, *Organometallics*, 2014, **33**, 1084–1099.
58 D. Braga, G. Cojazzi, D. Paolucci and F. Grepioni, *Chem. Commun.*, 2001, 803–804.
59 R. J. Webb, D. N. Hendrickson, M. D. Lowery, Y. Shiomi, M. Sorai and R. J. Wittebort, *Inorg. Chem.*, 1992, **31**, 5211–5219.
60 D. Braga, L. Scaccianoce, F. Grepioni and S. M. Draper, *Organometallics*, 1996, **15**, 4675–4677.
61 H. Kimata and T. Mochida, *Cryst. Growth Des.*, 2018, **18**, 7562–7569.
62 T. Mochida, Y. Funasako, M. Ishida, S. Saruta, T. Kosone and T. Kitazawa, *Chem.–Eur. J.*, 2016, **22**, 15725–15732.
63 T. Mochida, M. Ishida, T. Tominaga, K. Takahashi, T. Sakurai and H. Ohta, *Phys. Chem. Chem. Phys.*, 2018, **20**, 3019–3028.
64 H. Kimata, T. Sakurai, H. Ohta and T. Mochida, *ChemistrySelect*, 2019, **4**, 1410–1415.
65 J. Lin, P. Tong, K. Zhang, K. Tao, W. Lu, X. Wang, X. Zhang, W. Song and Y. Sun, *Nat. Commun.*, 2022, **13**, 596.
66 D. Braga and F. Grepioni, *Chem. Commun.*, 1996, 878–899.
67 T. Mochida, Y. Funasako, T. Inagaki, M. J. Li, K. Asahara and D. Kuwahara, *Chem.–Eur. J.*, 2013, **19**, 6257–6264.
68 F. Grepioni, G. Cojazzi, S. M. Draper, N. Scully and D. Braga, *Organometallics*, 1998, **17**, 296–307.
69 N. G. Connelly and W. E. Geiger, *Chem. Rev.*, 1996, **96**, 877–910.
70 G. Ferrer, C. Barreneche, A. Solé, I. Martorell and L. F. Cabeza, *J. Energy Storage*, 2017, **11**, 1–6.
71 B. H. Toby and R. B. Von Dreele, *J. Appl. Crystallogr.*, 2013, **46**, 544–549.
72 J. J. McKinnon, A. S. Mitchell and M. A. Spackman, *Chem.–Eur. J.*, 1998, **4**, 2136–2141.
73 J. M. Bermúdez-García, M. Sánchez-Andújar, S. Yáñez-Vilar, S. Castro-García, R. Artiaga, J. López-Beceiro, L. Botana, Á. Alegría and M. A. Señarís-Rodríguez, *Inorg. Chem.*, 2015, **54**, 11680–11687.
74 R. B. Woodward and M. Rosenblum, in *Ring Rotational Barrier in Ferrocene*, 1958, p. 5543.
75 K. Elihn and K. Larsson, *Thin Solid Films*, 2004, **458**, 325–329.
76 L. G. Domracheva, N. V. Karyakin, M. S. Sheiman, G. V. Kamelova, V. N. Larina, O. N. Suvorova and G. A. Domrachev, *Russ. Chem. Bull.*, 1999, **48**, 1647–1655.

77 O. V. Krol, A. I. Druzhinina, R. M. Varushchenko, O. V. Dorofeeva, M. D. Reshetova and N. E. Borisova, *J. Chem. Thermodyn.*, 2008, **40**, 549–557.
78 M. Sorai and Y. Shiomi, *Thermochim. Acta*, 1986, **109**, 29–44.
79 A. B. Bazyleva, G. J. Kabo and A. V. Blokhin, *Phys. B*, 2006, **383**, 243–252.
80 M. Bochmann, *Organometallics 1 – Complexes with Transitions Metal-Carbon σ-bonds*, Oxford University Press, 1994.
81 H. Hou, S. Qian and I. Takeuchi, *Nat. Rev. Mater.*, 2022, **7**, 633–652.
82 X. Moya, S. Kar-Narayan and N. D. Mathur, *Nat. Mater.*, 2014, **13**, 439–450.
83 J. Seo, R. D. McGillicuddy, A. H. Slavney, S. Zhang, R. Ukani, A. A. Yakovenko, S. L. Zheng and J. A. Mason, *Nat. Commun.*, 2022, **13**, 1–15.
84 P. Lloveras, E. Stern-Taulats, M. Barrio, J. L. Tamarit, S. Crossley, W. Li, V. Pomjakushin, A. Planes, L. Mañosa, N. D. Mathur and X. Moya, *Nat. Commun.*, 2015, **6**, 8801.
85 Materials for the Energy Transition roadmap, *Caloric Energy Conversion Materials*, 2020.

